PCCP

Formation of resonances and anionic fragments upon electron attachment to benzaldehyde

Journal:	*Physical Chemistry Chemical Physics*
Manuscript ID	CP-ART-01-2020-000029.R1
Article Type:	Paper
Date Submitted by the Author:	04-Mar-2020

Complete List of Authors:	Ameixa, Joao; CEFITEC, Physics; University of Innsbruck, Institute of Ion Physics and Apllied Physics Arthur-Baidoo, Eugene; Institute for Ion and Applied Physics, University of Innsbruck Pereira da Silva, Joao; CEFITEC, Physics Ryszka, Michal; The Open University Carmichael, Ian; University of Notre Dame Radiation Laboratory Cornetta, Lucas; Universidade de Sao Paulo Instituto de Fisica, Varella, Marcio; University of Sao Paulo, Physics Institute Ferreira da Silva, Filipe; CEFITEC - Centre od Physics and Technological Research, Physical Department FCT/UNL Ptasinska, Sylwia; University of Notre Dame Radiation Laboratory; University of Notre Dame, Department of Physics Denifl, Stephan; University of Innsbruck, Institute of Ion Physics and Apllied Physics

PAPER

Formation of resonances and anionic fragments upon electron attachment to benzaldehyde

Received 00th January 20xx,
Accepted 00th January 20xx

DOI: 10.1039/x0xx00000x

J. Ameixa,[ab] E. Arthur-Baidoo,[a] J. Pereira-da-Silva[b], M. Ryszka[c], I. Carmichael[c], L.M. Cornetta[d], M. T. do N. Varella[d], F. Ferreira da Silva[*b], S. Ptasińska[ce] and S. Denifl[*a]

Benzaldehyde is a simple aromatic aldehyde and has a wide range of applications in food, pharmaceutical, and chemical industry. The positive electron affinity of this compound suggests that low-energy electrons can be easily trapped by neutral benzaldehyde. In the present study, we investigated the formation of negative ions following electron attachment to benzaldehyde in the gas-phase. Calculations on elastic electron scattering from benzaldehyde indicate a π* valence bound state of the anion at –0.48 eV and three π* shape resonances (0.78, 2.48 and 5.51 eV). The excited state spectrum of the neutral benzaldehyde is also reported to complement our findings. Using mass spectrometry, we observed the formation of the intact anionic benzaldehyde at ~0 eV. We ascribe the detection of the benzaldehyde anion to stabilization of the π* valence bound state upon dissociative electron attachment to a benzaldehyde dimer. In addition, we report the cross sections for nine fragment anions formed through electron attachment to benzaldehyde. Investigations carried out with partially deuterated benzaldehyde show that the hydrogen loss is site-selective with respect to the incident electron energy. In addition, we propose several dissociation pathways, accounted by quantum chemical calculations on their thermodynamic thresholds. The threshold calculations also support that the resonances formed at higher energies lead to fragment anions observable by mass spectrometry, whereas the resonances at low electron energies decay only by electron autodetachment.

1. Introduction

Benzaldehyde (C_6H_5CHO, chart 1), is an aromatic aldehyde with a wide range of applications, mainly in the food industry as a flavouring agent or preservative. It may also serve as an important intermediate to produce various organic compounds, e.g., drugs, cosmetics, oils, inks, or plastics, thereby attracting the interest of the pharmaceutical and chemical industries.[1,2] Moreover, it also occurs spontaneously in alcoholic beverages, dairy products, meat, poultry, as well as in wide variety of fruits and vegetables.[3]

Benzaldehyde has chemotherapeutic relevance, which was proposed in late seventies by Takeuchi *et al.*.[4] Since then, benzaldehyde and its derivatives have been investigated and administrated to patients with advanced inoperable carcinomas without measurable toxicity.[4–7] The *in vitro* studies with human healthy and tumour cells have shown selective inhibition of the growth of the tumour cells without measured effects in the healthy cells.[6] Moreover, the combination of hyperthermia with benzaldehyde at doses that are nontoxic appears to enhance the cytotoxic effect.[8] Additionally, an *in vivo* assay further reports the inhibition by benzaldehyde of pulmonary metastasis in tumour-inoculated mice.[9] Even though, the underlying mode of operation of benzaldehyde at molecular level is still unclear. Aldehydes, including benzaldehyde, bound to cellular macromolecules in particular to the amino group of proteins forming Schiff's base adducts, may quench protein-mediated processes in the cell, for instance enzymes or the transport of molecules through the cell membrane.[10–12] Consequently, a hypothesis indicated that the anti-cancer effect by benzaldehyde is based on the inhibition of the uptake of essential nutrients, that are required for the growth of cancer cells.[13] In addition, another hypothesis suggested that the effect in cancer cells is associated with an efficient inhibition of glutathione peroxidase (GPx) by benzaldehyde, since GPx belongs to a family of enzymes that defend the organism from oxidative damage, leading to an increased production of highly reactive oxygen species (ROS), and consequently oxidative stress.[14,15] The latter species, in turn, e.g., $O_2^{\bullet-}$,$OH^{\bullet}$, $O^{\bullet}$, are harmful to DNA (free radical damage) and other biomolecules,

[a] Institut für Ionenphysik und Angewandte Physik and Center for Molecular Biosciences (CMBI), Leopold-Franzens Universität Innsbruck, Technikerstraße 25/3, 6020 Innsbruck, Austria. E-mail: Stephan.denifl@uibk.ac.at
[b] Atomic and Molecular Collisions Laboratory, CEFITEC, Department of Physics, Universidade NOVA de Lisboa, 2829-516 Caparica, Portugal E-mail:f.ferreiradasilva@fct.unl.pt
[c] Radiation Laboratory, University of Notre Dame, Notre Dame, Indiana 46556, USA
[d] Instituto de Física, Universidade de São Paulo, Rua do Matão 1731, 05508-090 São Paulo, Brazil
[e] Department of Physics, University of Notre Dame, Notre Dame, Indiana 46556, USA

† Electronic Supplementary Information (ESI) available: Thermodynamic thresholds calculated at the G4(MP2) (T=0K and T=298.15 K) for the observed anions, energy and width of the bound and resonant states obtained by SMCPP, and schematic diagram of the full active space used in the CASSCF/CASPT2 calculations. See DOI: 10.1039/x0xx00000x

thereby leading to mutations, cancer, and ultimately apoptosis.[16]

The ROS-induced DNA damage is also highly relevant in cancer radiotherapy. The ionisation of water following the interaction of high energy radiation with the cell tissue leads to the formation of ROS which may react with DNA, as well as to the production of a large amount of secondary low-energy electrons (LEEs), with an energy distribution peaking around 10 eV.[17–19] In this energy regime, LEEs may contribute to DNA damage, inducing mainly single- and double strand breaks, through dissociative electron attachment (DEA) reactions.[20,21] This process occurs when a molecule resonantly captures an electron forming a transient negative ion (TNI) that may decay into a anionic fragment and neutral radicals.[22–24]

The administration of radiosensitizers should enhance the sensitivity of tumours to high-energy radiation.[25] The related processes in the early physical-chemical stage of radiation damage are not fully understood yet. Recently, Meißner *et al.*[26] have shown that the first step of the radiosensitization of hypoxic tumour cells by the nitroimidazole relies on the efficient formation of the radical anion species by associative attachment of LEEs. In another way of radiosensitization, LEEs may induce the dissociation of electrophilic compounds, through DEA reactions yielding reactive radicals which are precursors for DNA damage. For instance, nucleobases/nucleosides with an electrophilic group at the C_5-position have been used as radiosensitizers.[27–29] These compounds exhibit a high reactivity towards LEEs due to a positive electron affinity (EA). Benzaldehyde has a EA of ~0.35 eV[30], thus it could serve as a radiosensitizer, although knowledge about the interactions of LEEs with benzaldehyde is limited. To the best of our knowledge, only two gas-phase studies on the interaction of LEEs with benzaldehyde have been carried out so far. Hacaloglu *et al.*[31] performed a DEA study with benzaldehyde, while Modelli *et al.*[32] have located shape resonances in benzaldehyde by electron transmission spectroscopy. The studies described by Hacaloglu et al.[31] show the most abundant anions formed through electron capture are O^-, and the phenyl anion. Moreover, the parent anion was not observed in their study. The experimental attachment energies determined by Modelli and Burrow[32] show two π* shape resonances at 2.21 and 4.34 eV in addition to a bound state.

To reach a better understanding of the interaction of LEEs with benzaldehyde, we have investigated the formation of anions through electron attachment by means of two experimental set-ups. In addition, we performed a detailed theoretical study by calculating elastic electron scattering cross sections, the electronic excitation spectra for neutral benzaldehyde, and also the thermodynamic thresholds for the formation of the observed anions. The present experimental results show the formation of the intact molecular anion via the dimer and the phenyl anion was observed as the most abundant fragment, in contrast to previous studies. Moreover, both computational chemistry and electron scattering calculations support our experimental results together with those from previous ETS experiments. Finally, we measured DEA to benzaldehyde-α-d1 (d-benzaldehyde) to clarify some dissociation pathways involving hydrogen loss.

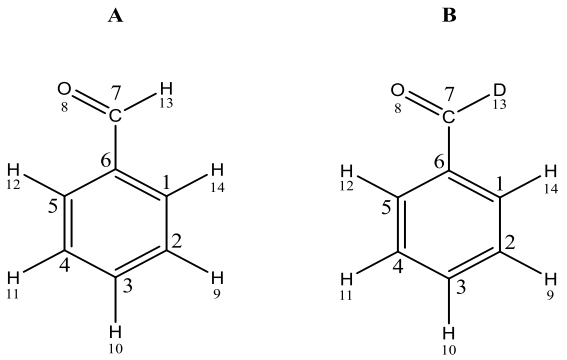

Chart 1 Chemical structure of (A) – benzaldehyde, (B) – benzaldehyde-α-d1 (d-benzaldehyde).

2. Methods

2.1 Experimental set-up

Benzaldehyde (106 u) was purchased from Sigma-Aldrich (stated purity ≥ 99%). The sample is a liquid at room temperature with a vapour pressure of 195.7 Pa.[33] It was purified by performing several freeze-pump-thaw cycles before performing the studies. In both experimental set-ups, the vapour of the liquid was introduced into an interaction region via a gas inlet coupled with a precision valve. At the University of Innsbruck, a crossed electron-molecular beam setup combined with a quadrupole mass spectrometer (QMS) was used. The setup was described in detail elsewhere.[34] Briefly, the sample's vapour enters into the interaction chamber of a hemispherical electron monochromator (HEM), through a 1 mm-diameter, stainless-steel capillary, where it crosses with an electron beam. The HEM was tuned to generate the electron beam with an energy resolution of 120 meV at full width at half maximum (FWHM) with an incident electron current of 10-30 nA. The formed anions are extracted towards the QMS by a weak electrostatic field from the interaction chamber and thus analysed by their mass-to-charge ratio. Finally, the mass-separated anions are detected by a channeltron-type secondary electron multiplier in a single-pulse counting mode. The presented ion yields were obtained by recording the intensity of a given mass-separated anion as a function of the incident electron energy. The electron energy scale and electron energy resolution were determined by measuring the well-known resonances for the formation of SF_6^- from SF_6 and Cl^- from CCl_4, at ~0 eV. Lastly, the electrons which pass the interaction region are collected by a Faraday plate and the obtained current is monitored by a picoammeter.

In this study, dissociative the electron attachment cross sections, σ_{DEA}, were determined by comparing the ion yields for the fragment anions formed from benzaldehyde with the well-known cross sections occurring at 0.8 eV for Cl^- from CCl_4 ($\sigma_{DEA}=5.0\times10^{-20}$ m^2)[35] or at 5.2 eV for F^- from SF_6 ($\sigma_{DEA}=5.0\times10^{-22}$ m^2).[36] For a given DEA reaction, the ion yields were corrected with the respect to the partial pressures of the

sample as well as the intensity of incident electron current at given experimental conditions. The experimental uncertainty of the determined cross-section values is within one order of magnitude.

At the Radiation Laboratory at the University of Notre Dame, the experiment consists of a high-vacuum chamber equipped with a QMS from Hiden Analytical, Inc. and it has been described previously.[37] First, the effusive molecular beam is directed towards the entrance of the QMS, by a 1 mm-diameter, stainless-steel capillary. Thereafter, the ions are formed by the interaction with electrons emitted by the internal filament (oxide-coated iridium wire) of the QMS. The anions are mass-analysed by the QMS and further detected by a channeltron. The ion yield for a particular anion was recorded as a function of the electron energy. The electron energy scale was calibrated by measuring the well-known resonances of SF_6^- and F^- from SF_6. The electron energy resolution was estimated to be approximately 500 meV (FWHM) for an incident electron current of 2 μA.

2.2 Computational methods

Apart from the scattering calculations and the electronic excitation spectra, all computations described below were performed with the Gaussian09 software package[38].

2.2.1 Geometry optimization

The ground state geometry of benzaldehyde was optimized with density functional theory (DFT), employing the hybrid functional B3LYP[39] and the aug-cc-pVTZ basis[40]. An essentially identical geometry was obtained with Møller-Plesset second-order perturbation theory (MP2) and the same basis. This geometry was employed in all calculations for the neutral and anion species, except for the vertical attachment energy (VAE) estimates obtained as empirically corrected virtual orbital energies (VOEs). In this case, the geometry and VOEs were calculated with the DFT/B3LYP/6-31G* method, following the prescription of Scheer *et al.*[41] .

2.2.2 Electron scattering calculations

We have employed the Schwinger Multichannel method[42,43] implemented with the Bachelet-Hamann-Schlüter[44] pseudopotentials (SMCPP). Details of the SMCPP variational approach to the collision problem and its implementation can be found elsewhere.[45] Here we briefly mention that the expansion of the scattering wave function in configuration state function (CSF) trial bases defines the static-exchange (SE) and SE plus polarization (SEP) approximations. The former employs CSFs given by $|\chi_{0\mu}\rangle = \mathcal{A}[|\Phi_0\rangle\otimes|\varphi_\mu\rangle]$, where $\mathcal{A}$ is the anti-symmetrization operator, $|\Phi_0\rangle$ is the target ground state obtained in the Hartree-Fock (HF) approximation, and $|\varphi_\mu\rangle$ is a scattering orbital. The SE scheme neglects correlation-polarization effects, which are accounted for by augmenting the SEP expansion with CSFs of the kind $|\chi_{\eta\nu}\rangle = \mathcal{A}[|\Phi_\eta\rangle\otimes|\varphi_\nu\rangle]$, where $|\Phi_\eta\rangle$ is a singly excited target state with either singlet or triplet spin coupling, although all CSFs are doublets. The construction of the CSF space was based on the energy criterion proposed elsewhere[40], which considers all configurations satisfying $\epsilon_{\text{particle}} + \epsilon_{\text{scattering}} - \epsilon_{\text{hole}} < \Delta$, where ϵ's correspond to the orbitals energies and Δ is an energy cutoff. We employed modified virtual orbitals generated from cationic cores with charge +2 and the cutoff $\Delta = -1.24$ Ha. The CSF space was also symmetry decomposed, such that the *A*'' component comprised 4824 trial basis functions in the SEP approximation. The SMCPP calculations were restricted to the *A*'' irreducible representation of the cross section, where the signatures of the π^* shape resonances should be evident. While σ^* resonances could also be expected for benzaldehyde, they are usually broad and embedded into the large background arising from the dipolar interaction, thus having no clear signatures in the calculated cross sections (unless heavier atoms are found[46,47]).

2.2.3 Dipole-bound states

The energy of the dipole bound state (DBS) was obtained according to Skurski *et al.*.[48] In brief, to account for the diffuse character of that state, the aug-cc-pVTZ basis was augmented with sets of 6s6p diffuse functions centred on the hydrogen atoms H(10) and H(11), located close to the positive end of the dipole moment vector (atomic labels shown in chart 1). The vertical DBS energy was computed with two methods, namely MP2 and coupled-clusters with single, double, and non-iterative triple excitations (CCSD(T)).

2.2.4 Thermodynamic thresholds

The dissociation thresholds for several channels were calculated at the B3LYP/aug-cc-pVTZ level of theory, firstly from enthalpy differences deduced from harmonic frequency calculations for a number of likely produced fragments, matching their masses with the observed mass-to-charge ratios. Based on these structures, enthalpies of formation for some selected fragments were further refined at the G4(MP2)[49] level of theory. In general, the zero-temperature thresholds are 0.2 - 0.5 eV lower than those obtained from enthalpy differences at room temperature (298.15 K).

2.2.5 Electronic excitation

The excited states of neutral benzaldehyde were calculated with the complete active space self-consistent field method and second-order perturbative corrections (CASSCF/CASPT2), as implemented in the OpenMOLCAS[50] software package. The calculations employed the ANO-L basis set with the contraction scheme [4s3p1d] for carbon and oxygen atoms, and [2s1p] for the hydrogens. This basis set was calibrated for describing valence excited states at CASPT2 level[51] and it have been employed for some systems in previous studies of neutral and anionic species[52,53]. The (12,10) active space comprised 12 electrons and 10 active orbitals in the reference HF ground state, namely four π-type and two n-type occupied orbitals, along with four π^* virtual orbitals. The same orbital space was employed for the anion, the only difference being the number of active electrons, (13,10). The occupied orbitals are labelled, from the (HOMO-5) to the HOMO level, as π_4, n_2, π_3, n_1, π_2, π_1, while the unoccupied ones, from the LUMO to the LUMO+3 level, as π^*_1 to π^*_4.

3. Results and discussion

3.1 Electron scattering calculations

The *A''* symmetry component of the integral cross section (ICS), obtained in both the SE and SEP approximations for elastic electron scattering is presented in figure 1. The SE calculations show four shape resonances at 1.59, 2.65, 4.98 and 9.63 eV, which are labelled π_1^* to π_4^* in order of increasing energy. Virtual orbital plots generated with compact basis sets (HF/6-31G*) are also shown to provide insight into the characters of the anion states. The inclusion of polarization effects (SEP approximation) shifts the resonances to lower energies, as expected, and the lowest lying π_1^* state becomes stable. The diagonalization of the scattering Hamiltonian represented in the CSF space indicates a valence bound state (VBS) at –0.48 eV (the energies of bound and resonance states are indicated as negative or as positive, respectively). From more sophisticated CCSD/aug-cc-pVDZ calculations, we obtained a vertical binding energy of –0.31 eV for the π_1^* anion state, which is in good agreement with the DFT estimation (~ –0.35 eV) reported by Buonaugurio *et al.*.[30] In the SEP cross section, the higher lying π^* anion states are resonances located at 0.78, 2.48 and 5.51 eV. The positions and widths of the resonances are presented in Table I, along with the empirically corrected VOEs, and the electron transmission spectroscopy (ETS) values reported by A. Modelli *et al.*.[32] There is good agreement between the SMCPP calculations and the experimental data, except for the π_4^* state. The discrepancy for the latter state is not surprising, since elastic scattering calculations, which neglect electronic excitations channels, often overestimate the energy of higher lying π^* anion states with mixed shape and core-excited character, by 0.5 to 1 eV (see Kossoski *et al.*[46] and references therein).

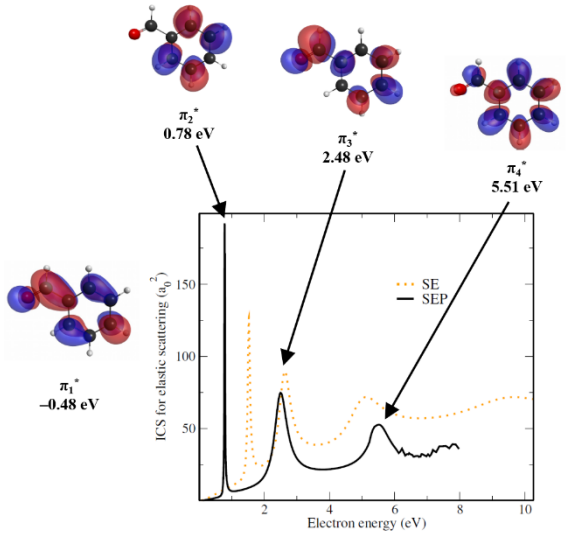

Fig. 1 A'' symmetry component of the elastic integral cross section (ICS). The dotted line corresponds to the SE approximation, while the solid line to the SEP results. The energies of the π^* resonances are indicated in the panel for the SEP calculations (π_1^* is a valence bound state, not represented in the graph). Virtual orbital plots calculated with compact basis sets are also shown to provide insight into the bound and resonance characters.

Table I Positions and widths (given in parenthesis) of the shape resonances of benzaldehyde (in eV). We show the results obtained with the SMCPP method and the scaled VOEs calculated with the empirical scaling relation of Scheer *et al.*.[41] The ETS data of Modelli *et al.*[32] is also indicated for comparison.

	π_1^*	π_2^*	π_3^*	π_4^*
SMCPP	-0.48	0.78 (0.024)	2.48 (0.48)	5.51 (0.78)
Scaled VOEs	-0.46	0.61	1.79	4.43
ETS data[32]	< 0	0.71-0.85	2.21	4.34

3.2 Excited states for neutral benzaldehyde (0 - ~ 9.5 eV)

We calculated the electronic excitation spectrum of neutral benzaldehyde with the CASSCF/CASPT2 method. While we did not include electronic excitation channels in the scattering calculations, the energy of the excited triplet and singlet states of the target molecule might be of help in assigning a type of core-excited resonances. The calculated values are shown in Table II for energies up to 8.2 eV (the ionisation potential is 9.5 eV[54]). The dominant character of the excitations is also indicated whenever they could be clearly identified.

Table II Vertical electronic states for neutral benzaldehyde obtained at the CASSCF/CASPT2 level of theory. S and T stand for singlet and triplet spin states, respectively.

Electronic state (neutral)	Energy (eV)
S_0	0.00
$T_1(n_1 \rightarrow \pi_1^*)$	3.57
$S_1(n_1 \rightarrow \pi_1^*)$	3.83
$T_2(\pi_1 \rightarrow \pi_1^*)$	3.85
$T_3(\pi_2 \rightarrow \pi_1^*)$	4.18
$T_4(\pi_2 \rightarrow \pi_2^*)$	4.70
$T_5(\pi_1 \rightarrow \pi_2^*)$	4.80
$T_6(\pi_3 \rightarrow \pi_1^*)$	5.77
$S_2(\pi_1 \rightarrow \pi_1^*)$	5.93
$T_7(n_1 \rightarrow \pi_2^*)$	6.07
$S_3(n_1 \rightarrow \pi_2^*)$	6.30
T_8	6.42
T_9	6.54
S_4	6.69
S_5	6.73
$T_{10}(\pi_4 \rightarrow \pi_1^*)$	7.14
S_6	7.58
$T_{11}(\pi_2,n_1 \rightarrow \pi_1^*, \pi_2^*)$	8.05
S_7	8.19

3.3 Electron attachment to benzaldehyde

Table III summarizes the observed anions and positions of the maxima for each ion yield together with the calculated thermodynamic thresholds. Ten different anions were identified, all are formed at energies above 3.6 eV except the benzaldehyde anion formed at ~0 eV. The lowest thermodynamic threshold for DEA to benzaldehyde lies at 2.53 eV corresponding to the formation of $C_6H_5^-$. Consequently, the shape resonances π_2^* and π_3^* identified here by the electron scattering calculations at 0.78 and 2.48 eV (see Section 3.1) are unlikely precursors for DEA to benzaldehyde, since the measured onsets for the formation of fragment anions occur at much higher energies. Therefore, the shape resonances π_2^* and π_3^* decay via autodetachment. The DEA cross sections are also depicted in Table III.

Hacaloglu *et al.*[31] studied electron attachment to a collection of unsaturated carbonyls, including benzaldehyde, by means of a crossed-beam experiment comprising a trochoidal electron monochromator coupled with a QMS. Since experimental details, such as the incident electron current, electron energy resolution, calibration method for the electron energy scale and the working pressure were not mentioned in their work,[31] we omit a comprehensive comparison with our results. To briefly summarize their study, the authors have reported a total of seven anionic fragments. Six of them had the onset above 6.6 eV while the onset for the formation of $C_6H_5^-$ was 1.5 eV. The latter value is substantially lower than the presently predicted thermodynamic threshold of 2.53 eV. Other major differences to the present results are related to the shape of the ion yields as well as relative intensities of fragment anions. For example, O^- was observed as most abundant fragment anion in their work.[31]

3.3.1 Formation of the benzaldehyde anion

Figure 2 shows the ion yield for the intact benzaldehyde anion, *m/z* 106 $C_6H_5CHO^-$ (M), measured with the HEM instrument. The ion yield shows a narrow peak close to 0 eV electron energy and other structures between 6 and 10 eV. The higher energy features are assigned to the dehydrogenated benzaldehyde anion, $(M–H)^-$, due to the isotopic contributions. We also studied the dependence of the ion yield at *m/z* 106 as function of the working pressure of benzaldehyde in the chamber. The pressure range was between 5.4×10^{-5} and 1.3×10^{-4} Pa. At the lowest pressure, 5.4×10^{-5} Pa, the intensity of the ion yield measured at ~0 eV is comparable with the high-energy features of the $(M–H)^-$; while at higher pressures, the ion yield at ~0 eV starts to dominate. In general, any elevated pressure in the capillary may induce the formation of benzaldehyde dimers. It is well-known that benzaldehyde molecules can efficiently form linear and cyclic dimers, via intermolecular hydrogen bonds, C=O---H–C, between the oxygen of a given benzaldehyde molecule and the H atom within the formyl moiety of a neighbouring molecule.[55] At higher pressure, the neutral density of dimers of benzaldehyde in the collision chamber is expected to be enhanced. Consequently, the intact benzaldehyde anion may form upon DEA to a dimer, as suggested by the pressure dependence on the ion yield obtained at ~0 eV (reaction (1)). Furthermore, due to its electron affinity, benzaldehyde admits a VBS (π_1^*) that lies ~0.48 eV below the ground state of the neutral. The respective singly occupied orbital of the VBS is shown in figure 3-a). The

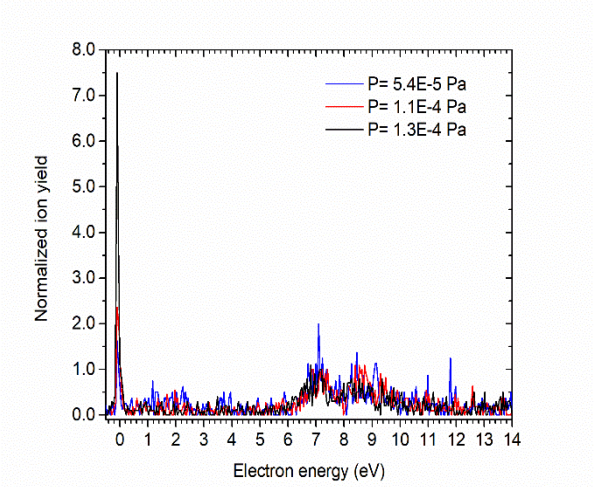

Fig. 2 Ion yield of $C_6H_5CHO^-$ measured at different working pressures in the HEM instrument. The ion yields were normalized with respect to the maxima of the signal at ~7.13 eV.

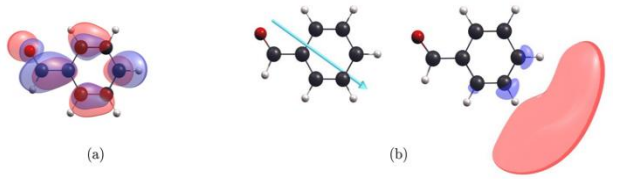

Fig. 3 (a) SOMO of the valence bound state (VBS) of the anion (A'' symmetry), (b) the permanent dipole moment vector of the neutral and the SOMO of the DBS (A' symmetry).

experimental detection of the intact benzaldehyde anion is thus associated with an effective stabilization of the VBS by excision of the other benzaldehyde unit.

Under comparable pressures, the benzaldehyde anion was not observed in the study performed with the Notre Dame instrument. It is important to note that, when compared to the HEM instrument, the distinct characteristics of the ion source, e.g., physical dimensions, a lower electron current close to 0 eV, the fact that the effusive beam is directed towards the hot filament, or the lower detection limit of the instrument, can influence the possibility of dimer formation and stability prior to electron interactions and thus the observation of the benzaldehyde anion. Nevertheless, besides the anionic monomer, we rule out that any further fragment anions are formed from DEA to dimers, since the neutral dimer density is very low. Furthermore, this is the only anion observed at ~0 eV, where the s-wave electron attachment cross section achieves its maximum[56].

$$(C_6H_5CHO)_2 + e^-(\sim 0eV) \rightarrow (C_6H_5CHO)_2^{\#-} \rightarrow C_6H_5CHO^- + C_6H_5CHO \quad (1)$$

Table III Mass-to-charge ratio (*m/z*) of the observed anionic fragments formed upon electron attachment to benzaldehyde, as well as measured DEA cross sections along with the respective resonance positions, sorted by increasing energy, and experimental thresholds. Thermodynamic thresholds were calculated at the G4(MP2) (indicated with [a]) or at B3LYP/aug-cc-pVTZ (indicated with [b]) levels of theory.

			Resonance Position (eV)			Threshold (eV)		
m/z	**Anion**	σ_{DEA} ($\times 10^{-24}$ m^2)	**1.**	**2.**	**3.**	**Exp.**	**Theory**	
106	$C_6H_5CHO^-$		~0			~0		
							C_1–H(14)	2.98[a]
							C_2–H(9)	2.92[a]
105	$[C_6H_5CHO\text{-}H]^-$	9.85	4.6	7.6	9.2	3.6	C_3–H(10)	2.83[a]
							C_4–H(11)	2.86[a]
							C_5–H(12)	2.68[a]
							C_7–H(13)	2.80[a]
90	$C_6H_5CH^{\bullet -} + O(^3P)$ $C_6H_5CH^{\bullet -} + O(^1D)$	3.84	7.4			5.9	5.92[a] 7.97[a]	
89	$C_6H_5C^-$	31.1	6.9	7.6		6.2	5.41[a]	
88	$C_6H_4C^-$	15.8	6.8			5.9	2.92[a]	
77	$C_6H_5^-$	95.8	4.7	6.5	7.0	3.8	2.53[a]	
62	HC_5H^-	3.35	8.1			6.5	4.1[b]	
49	C_4H^-	3.01	8.2			6.4	5.5[b]	
17	OH^-	46.1	7.3	8.3	9.7	6.4	4.72[a]	
16	O^-	23.5	7.8	8.9	10.5	6.5	6.02[a]	

3.3.2 Dehydrogenated benzaldehyde anion

The DEA reaction (2) represents the formation of the dehydrogenated benzaldehyde anion. In figure 4, the ion yield shows a weak contribution at 4.6 eV which we assign to the π_4^* resonance with mixed shape/core-excited character. The two higher-lying contributions centred at 7.6 and 9.2 eV are assigned as core-excited resonances. The estimated cross section for formation the dehydrogenated benzaldehyde anion is 9.85×10^{-24} m^2. This small value indicates the low effectiveness of this fragmentation channel.

$$C_6H_5CHO + e^- \rightarrow C_6H_5CHO^{\#-} \rightarrow (C_6H_5CHO\text{-}H)^- + H \quad (2)$$
$$C_6H_5CDO + e^- \rightarrow C_6H_5CDO^{\#-} \rightarrow (C_6H_4CDO\text{-}H)^- + H \quad (3)$$

The dehydrogenation of biomolecules upon DEA has been described for several nucleobases.[57–59] The experimental and theoretical studies carried out with thymine and uracil suggest that the dehydrogenation proceeds through a dipole-bound state (DBS)[58,59] where an incoming electron is temporally captured. Therefore, we also investigated DBS as a possible doorway state for hydrogen loss by benzaldehyde. According to the DFT/B3LYP/aug-cc-pVDZ calculations, neutral benzaldehyde has a dipole moment around 3.6 D, and thus expected to hold a DBS[60]. Both the MP2 and CCSD(T) calculations performed with the diffuse basis sets seems to indicate very shallow DBSs, with binding energies of 1 meV and 2 meV, respectively. We note that the binding energies lie within the uncertainty of the calculations. In figure 3-b), we show that the positive pole of the permanent dipole moment vector of the neutral is lying on the hydrogens H(10) and H(11) as well as the DBS single occupied molecular orbital (SOMO).

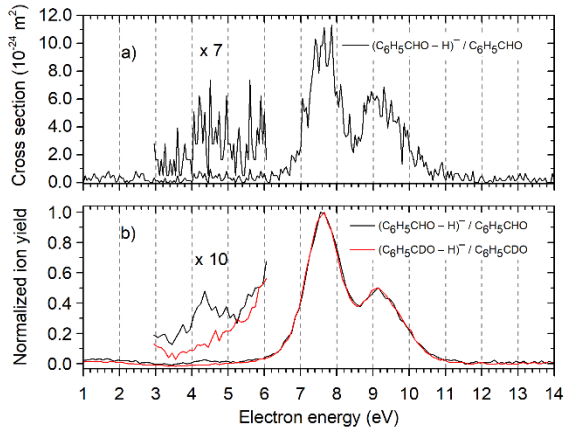

Fig. 4 Negative ion yields for the dehydrogenated benzaldehyde. a) Cross section for the formation of the dehydrogenated benzaldehyde anion from benzaldehyde measured with the HEM instrument. b) Dehydrogenated parent anion formation from benzaldehyde (black) and d-benzaldehyde (red) measured with the Notre Dame instrument. The ion yield was normalized with respect to the maxima of the signal at 7.6 eV.

The calculated thermodynamic threshold values at the G4(MP)2 level of theory are listed in Table III for the loss of hydrogen from the distinct positions in benzaldehyde. The theoretical calculations show that hydrogen loss from benzaldehyde is always an endothermic reaction, even though the dehydrogenation from the phenyl moiety (C_5 position) appears to be energetically more favourable. Usually, the electron-induced dissociation mediated by a DBS gives rise to low-lying structures (<3 eV) in the ion yield of the dehydrogenated parent anion measured from uracil, thymine[58], adenine[61,62] and their derivatives (OTfU[63] and 2-chloroadenine[64]), as well as 3-bromopyruvic acid[65]. In the case of benzaldehyde, however, such structures are not observable in the ion yield shown in Figure 4. It suggests that the DBS does not play a role as a doorway state for the loss of hydrogen upon electron attachment, since the experimental onset for the observed dehydrogenated benzaldehyde anion occurs at ~3.6 eV, which is much higher than those for hydrogen loss in uracil, thymine, and their derivatives, due to the lack of strong polar N–H bonds. Furthermore, the experimental threshold is also too high in the energy scale of C–H vibrational excitation, which is typically ~0.4 eV for infra-red active modes. Thus, even if vibrational Fesbach resonances (VFRs) are formed, we expect that it would be very unlikely that there would be a high enough tunnelling barrier to give rise to long-lived VFRs at such high energies.

The mentioned experimental onset lies above the calculated thermodynamic threshold for all hydrogen positions, which hinders the assignment of the dehydrogenation site to a particular position. Therefore, we investigated the dehydrogenation upon DEA to deuterated benzaldehyde-α-d_1 (d-benzaldehyde) to clarify the abstraction of hydrogen. Figure 4-b) shows the dehydrogenated parent anion formation from DEA to d-benzaldehyde, as described by reaction (3). The intensity was normalized with respect to the maximum of the signals, at 7.6 eV. While the two structures at ~7.6 and ~9.2 eV are common for both compounds, the weak structure at 4.6 eV is suppressed completely in d-benzaldehyde. The suppression of this channel can be explained in terms of autodetachment as a result of the slower dissociation dynamics due to presence of deuterium. The dehydrogenation from the C_7 position is thus triggered by ~4.6 eV electrons. The selectivity of H loss from benzaldehyde upon electron capture is then reachable by a proper tuning of the incident electron energy. The present observations support the rationale of DEA as a non-statistical dissociation process.[66]

3.3.3 Stripping off the formyl group

The phenyl anion, $C_6H_5^-$, together with the neutral counterpart formyl $CHO^\bullet$ are formed through the cleavage of the C_6–C_7 bond upon DEA to benzaldehyde, as described by reaction (4). The anion yield exhibits a peak centred at about 4.7 eV which arises from the π_4^* resonance. It is followed by a sharply rising feature at about 6.5 eV, having an asymmetric shape that suggests a shoulder at around 7.0 eV (figure 5-a)). These two contributions result from core-excited resonances within the energy range for electronic excitation. The phenyl anion stands as the most abundant anion with a maximum cross section of about 95.8×10^{-24} m^2 at 6.5 eV.

$$C_6H_5CHO + e^- \rightarrow C_6H_5CHO^{\#-} \rightarrow C_6H_5^- + CHO^\bullet \quad (4)$$

$$C_6H_5CDO + e^- \rightarrow C_6H_5CDO^{\#-} \rightarrow C_6H_5^- + CDO^\bullet \quad (5)$$

$$\rightarrow C_6DH_4^- + CHO^\bullet \quad (6)$$

The figure 5-b) shows the phenyl anion formation from DEA to d-benzaldehyde, as described by reaction (5), along with the ion yield detected at *m/z* 78. The formation of the phenyl anion

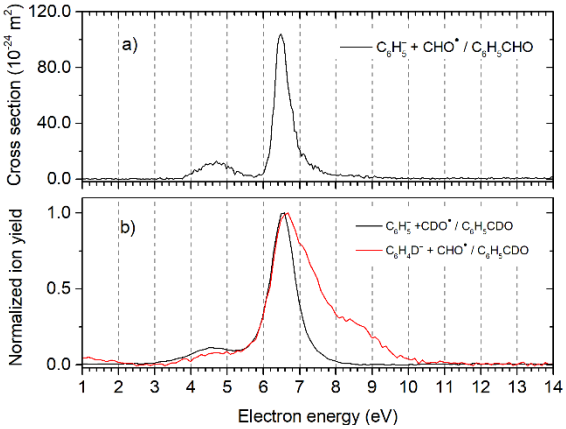

Fig. 5 a) Cross section for the formation of the phenyl anion, *m/z* 77 $C_6H_5^-$, from benzaldehyde measured with the HEM instrument. b) (Black) Formation of the phenyl anion from d-benzaldehyde, and formation of the deuterated phenyl anion, *m/z* 78 $C_6H_4D^-$, from d-benzaldehyde (in red) measured with the Notre Dame instrument. The ion yield was normalized with respect to the maxima of both signals.

either from benzaldehyde or d-benzaldehyde occurs at the same electron energies. This anion of m/*z* 78 formed by reaction (6) is assigned to $C_6H_4D^-$. It is formed not only through resonances centred at 4.7 and 6.5 eV resonances, but also through higher-lying contributions at 7.5 and 8.5 eV. Its formation involves an internal rearrangement exchanging the deuterium atom from the formyl group with hydrogen from the phenyl moiety, or due to a reaction involving ring opening. The four contributions may be attributed to these fragmentation mechanisms. The positions were determined by fitting the ion signal with Gaussian functions (please see figure S2 in the ESI).

3.3.4 Cleavage of the C=O bond: Loss of O•

The $C_6H_5CH^-$ anion is formed by the cleavage of the C=O bond, as described by DEA reaction (7). This reaction yields the reactive oxygen radical, O• as a neutral. $C_6H_5CH^-$ is observed through a single core-excited resonance centred at 7.4 eV with a maximum cross section of about 3.84×10^{-24} m^2 (figure 6). We report two thermodynamic thresholds which differ by the spin multiplicity of the oxygen atom, i.e. ~5.9 eV for triplet O(^{3}P) and ~8.0 eV for doublet O(^{1}D). Hence, the experimental onset of 5.9 eV agrees with the neutral release of the triplet oxygen atom upon electron attachment to benzaldehyde. O^- is formed through a core-excited resonance with a cross section of about 23.5×10^{-24} m^2 peaking at 8.9 eV (reaction (8)). The asymmetric shape of the feature seems to indicate two further contributions centred at about 7.8 and 10.5 eV (figure 6). The experimental onset of about 6.5 eV is in line with the predicted thermodynamic threshold of 6.02 eV for the formation of O^-.

$$C_6H_5CHO + e^- \rightarrow C_6H_5CHO^{\#-} \rightarrow C_6H_5CH^- + O^\bullet \quad (7)$$

$$\rightarrow O^- + C_6H_5CH \quad (8)$$

3.3.5 Concomitant cleavage of the C=O and C–H bonds: Loss of OH•

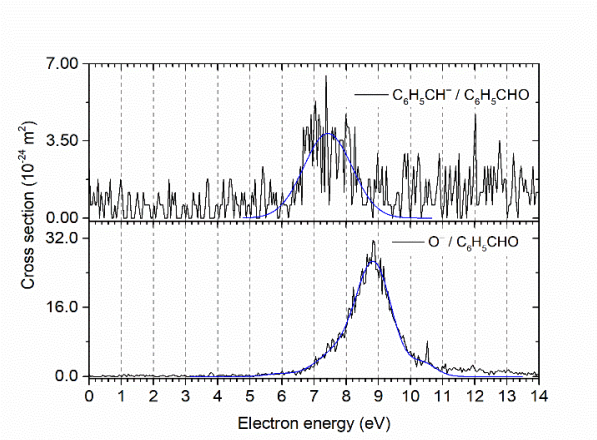

Fig. 6 Cross section for the formation of $C_6H_5CH^-$ (top) and O^- (bottom) through DEA to benzaldehyde. The blue line corresponds to the convoluted Gaussian fit to guide the eye.

The formation of $C_6H_5C^-$ and the radical OH• occurs through a core-excited resonance with a cross section of about 31.1×10^{-24} m^2 peaking at 6.9 eV, as represented by reaction (9). The shoulder may suggest a weaker contribution at 7.6 eV (figure 7). We predicted thermodynamic thresholds for loss of OH• by considering the position of the hydrogen atom involved in the reaction. The dehydrogenation from the formyl moiety (C_7 position) with further recombination with neutral oxygen arises as the thermodynamically most favourable reaction. The threshold for this reaction was estimated as 5.41 eV which is below the experimental threshold of 6.2 eV. On the other hand, when the dehydrogenation occurs from the phenyl moiety the respective thermodynamic thresholds are higher and range from 5.41 eV up to 6.15 eV (Table SII in the ESI).

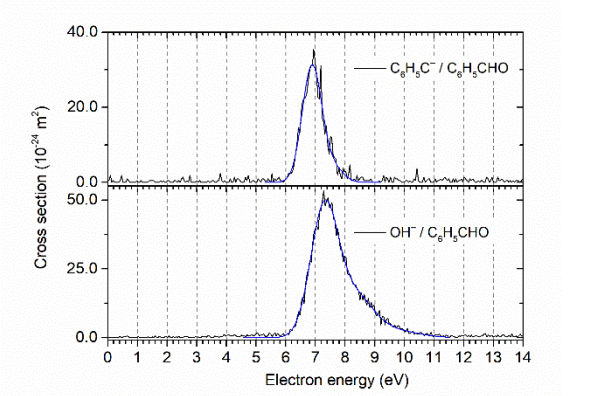

Fig. 7 Cross section for the formation of $C_6H_5C^-$ (top), and OH^- (bottom) through DEA to benzaldehyde. The blue line corresponds to the convoluted Gaussian fit to aid the eye.

$$C_6H_5CHO + e^- \rightarrow C_6H_5CHO^{\#} \rightarrow C_6H_5C^- + OH^\bullet \quad (9)$$

$$\rightarrow OH^- + C_6H_5CH^\bullet \quad (10)$$

The hydroxide anion (OH^-) is formed via reaction (10) where $C_6H_5C^\bullet$ is generated as a neutral radical. The ion yield shows a core-excited resonance with a maximum cross section of about 46.1×10^{-24} m^2 occurring at 7.3 eV (figure 7). Furthermore, the slow decay of the signal may imply two further contributions at 8.3 and 9.7 eV. The thermodynamic threshold was also predicted by considering the various positions for dehydrogenation. The lowest threshold of 4.72 eV is obtained when the dehydrogenation occurs from the formyl group (C_7 position), similarly to the complementary anion, $C_6H_5C^\bullet$. The experimental threshold of 6.4 eV lies above the predicted thermodynamic threshold in all cases. The further thresholds for this reaction range from 4.72 up to 5.98 eV and are presented in the Table SII in the ESI. Moreover, the ion yields of the above-mentioned DEA reactions show structures occurring at about the same electron energy, which suggests that a common electronic state of the TNI undergoes a structural rearrangement to give OH^- or $C_6H_5C^-$ from benzaldehyde.

3.3.6 Loss of H_2O

H_2O/(OH+H)/(O+H+H) is the neutral counterpart of the anion $C_6H_4C^-$. The ion yield for the formation of $C_6H_4C^-$ shows a single

core-excited resonance with a maximum cross section of 15.8×10^{-24} m^2 peaking at 6.8 eV, as described by reaction (11) and shown in figure 8-a). This anion arises from rearrangement following DEA to benzaldehyde; therefore, we have investigated several possibilities for fragmentation and symmetry arguments were used to compact the threshold predictions. The Table SII in the ESI summarizes the thermodynamic thresholds which lead to the formation of $C_6H_5C^-$ along with water elimination. The experimental onset of about 5.9 eV lies above the calculated thermodynamic thresholds in all cases, which does not allow a clear assignment. However, the lowest thermodynamic prediction of 2.92 eV for water elimination upon DEA to benzaldehyde suggests the

$$C_6H_5CHO + e^- \rightarrow C_6H_5CHO^{\#-} \rightarrow C_6H_4C^- + H_2O \quad (11)$$

$$C_6H_5CDO + e^- \rightarrow C_6H_5CDO^{\#-} \rightarrow C_6H_4C^- + HDO \quad (12)$$

$$\rightarrow C_6H_3CD^- + H_2O \quad (13)$$

recombination of hydrogen and oxygen from the formyl moiety (C_7 position) together with an additional hydrogen from either C_5 or C_1 positions within the phenyl moiety.

The figure 8-b) shows the formation of *m/z* 88 $C_6H_4C^-$ with loss of semi-heavy water (HDO). The ion yield, represented in black, shows features occurring at 6.5 and 8.5 eV. The neutral HDO appears to be formed from dehydrogenation from a position within the phenyl moiety along with a recombination with the deuterium and oxygen atoms from the formyl group (reaction 12). The anion detected at *m/z* 89 is assigned as $C_6H_3CD^-$ formed with loss of neutral water upon DEA to d-benzaldehyde (reaction 13). The ion yield of *m/z* 89 $C_6H_3CD^-$ also shows a contribution at ~6.5 eV. Its formation involves the reaction of a hydrogen atom removed from a position within the phenyl group, with deuterium from the formyl group. This anion may have a linear structure resulting from ring opening. However, from the current standpoint, in terms of experimental and theoretical approaches, we cannot describe the structure in detail.

3.3.7 Ring opening

Anionic pentadiynylidene, HC_5H^-, is formed through a single core-excited resonance with a maximum cross section of about 3.35×10^{-24} m^2 at 8.1 eV, as shown in figure 9. The possible thermodynamic thresholds, E_{Thr}, for the DEA reactions that may lead to the formation of HC_5H^- are predicted, as follows:

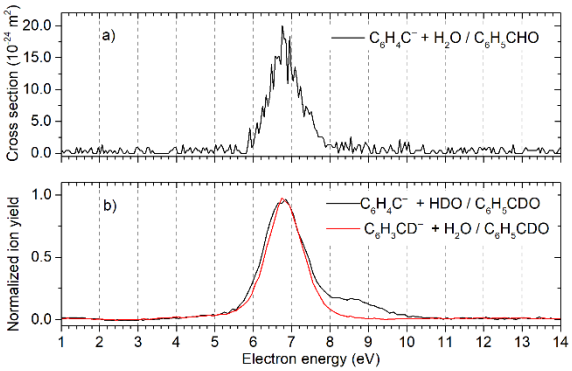

Fig. 8 a) Cross section for the formation of $C_6H_4C^-$ with loss neutral water, from benzaldehyde measured with the HEM instrument. b) Formation of $C_6H_4C^-$ with loss of semi-heavy water (HDO) from d-benzaldehyde (in black) and formation of $C_6H_3CD^-$ with loss of neutral water from d-benzaldehyde (in red) measured with the Notre Dame instrument. The ion yield was normalized with respect to maxima of the signal, respectively.

$$C_6H_5CHO + e^- \rightarrow C_6H_5CHO^{\#-}$$

$$\rightarrow HC_5H^- + CH_3 + CHO \quad E_{Thr} = 7.50\ eV \quad (14)$$

$$\rightarrow HC_5H^- + H_2C{=}C{=}O + H_2 \quad E_{Thr} = 5.20\ eV \quad (15)$$

$$\rightarrow HC_5H^- + CH_3CHO \quad E_{Thr} = 4.10\ eV \quad (16)$$

The DEA reaction (14) describes the formation of HC_5H^- alongside both methyl and formyl groups as neutrals. However, in this case, both neutral products recombine during the DEA process generating neutral acetaldehyde. For this pattern, the thermodynamic threshold of 7.5 eV is thus reduced to 4.1 eV, as described by reaction (16). On the other hand, reaction (15) that considers a distinct set of neutral byproducts, such as ketene (H2C=C=O) and molecular hydrogen has a thermodynamic threshold of 5.2 eV. Consequently, at the onset of the measured ion yield (6.5 eV), only the dissociation pathways described by reactions (15) and (16) are energetically accessible. Further studies, namely stepwise electron spectroscopy[24], would be required in order to experimentally characterize the HC_5H^- upon DEA to benzaldehyde.

The anion C_4H^- is also formed through a single core-excited resonance with a maximum cross section of 3.01×10^{-24} m^2 at 8.2 eV, as shown in figure 9. The formation of this anion may involve complex fragmentation within the molecule, similarly as suggested for HC_5H^-; and follows via:

$$C_6H_5CHO + e^- \rightarrow C_6H_5CHO^{\#-}$$

$$\rightarrow C_4H^- + C_2H_4 + CHO \quad E_{Thr} = 5.60\ eV \quad (17)$$

$$\rightarrow C_4H^- + C_3H_3O + H_2 \quad E_{Thr} = 5.50\ eV \quad (18)$$

The DEA reactions (17) and (18) that represent the formation of C_4H^- possess closely lying thermodynamic thresholds, although the considered neutral by products are different. The reaction (17) considers the formation of ethene and formyl as neutrals, while the reaction (18) considers C_3H_3O and molecular hydrogen. The experimental onset for the formation C_4H^- is about 6.4 eV, which is higher than both thermodynamic thresholds. Finally, it should be noted that the anions $C_4H^-$and HC_5H^- display a contribution centred at the same electron energy, which is an evidence that both anionic species may share an electronic state of the TNI.

4. Conclusions

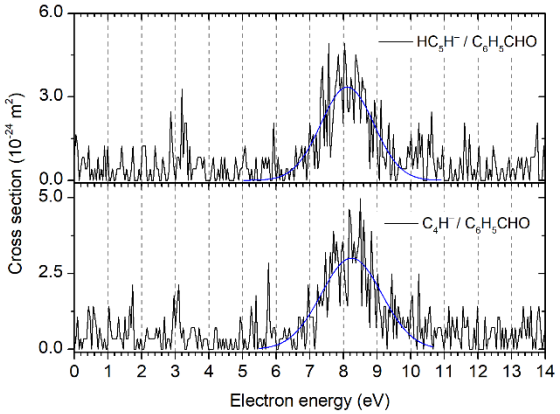

Fig. 9 Cross section for the formation of HC_5H^- (top) and C_4H^- (bottom) through DEA to benzaldehyde. The blue line corresponds to the convoluted Gaussian fit to aid the eye.

In the present studies we have comprehensively investigated electron attachment to benzaldehyde with three different approaches, namely mass spectrometry, electron scattering and quantum chemistry calculations. This combination provides in-depth analysis of benzaldehyde's fragmentation, since mass spectrometry allowed the identification of long-lived charged species, while the scattering calculations provide the short-lived states. Furthermore, the quantum chemistry study gives insight into the dissociation reactions and neutral products.

The formation of the intact benzaldehyde anion at energies close to 0 eV occurs via DEA to the dimer. This process is associated with an effective stabilization of the valence bound state π_1* of the anion. The rich fragmentation pattern comprises ten fragment anions formed with modest DEA cross sections peaking at relatively higher energies. Further, the lower lying resonances found by theoretical calculations do not result in DEA due to thermodynamic barriers for predicted fragmentation patterns. Therefore, these resonances can only decay by electron autodetachment.

Because the phenyl moiety in benzaldehyde resembles benzene, similarly to the present study, three π* shape resonances where identified for benzene using the SMCPP method[67]. The first two resonances have been pointed out as degenerated and occurring at ~1.4 eV, while the third resonance occurs at ~4.9 eV. The presence of the formyl moiety in benzaldehyde breaks the degeneracy of the two first π* states, estimated here at 0.78 and 2.48 eV. The same characteristic was noted previously for further benzene-related compounds, such as phenol, by using the same method.[68]

The study with d-benzaldehyde clarified that H loss from benzaldehyde is remarkably selective with respect to the incident electron energy, where the π_4* shape resonance at 4.6 eV is suppressed upon deuteration of the formyl moiety, while the higher-lying core-excited resonances are preserved for both compounds.

In conclusion, the results obtained here deliver a comprehensive description of the low-energy electron-induced dissociation of benzaldehyde and may thus contribute to a better knowledge of this compound for medical applications such as anti-cancer therapies. The electron-induced loss of $O^•$, $OH^•$ and a collection of further radicals and anions seems to suggest that anti-cancer effect of benzaldehyde may be enhanced in concomitant radio- and chemotherapy, though further studies, e.g., in aqueous solution or in water clusters, are required in order to model cellular conditions.

5. Conflicts of interest

There are no conflicts to declare.

Acknowledgements

JA and JPS acknowledge the Portuguese National Funding Agency FCT-MCTES through grants PD/BD/114447/2016 and PD/BD/142768/2018 respectively. FFS acknowledge the research grant PTDC/FIS-AQM/31215/2017. This work was also supported by Radiation Biology and Biophysics Doctoral Training Programme (RaBBiT, PD/00193/2012); UIDB/04378/2020 (UCIBIO); UIDB/00068/2020 (CEFITEC). SD acknowledges support from the FWF, Vienna (P30332). IC and SP are supported by the US Department of Energy Office of Science, Office of Basic Energy Sciences under Award Number DE- FC02-04ER15533. This is contribution number NDRL 5266 from the Notre Dame Radiation Laboratory. MTNV and LMC acknowledge support from the São Paulo Research Foundation (FAPESP, Grant No. 2015/17273-5 and 2017/24145-9. MTNV also acknowledges the Brazilian National Council for Scientific and Technological Development (CNPq), Grant No. 304571/2018-0. The calculations were partly performed with HPC resources from STI at the University of São Paulo.

Notes and references

1 E. Demir, S. Kocaoğlu and B. Kaya, *Food Chem. Toxicol.*, 2010, **48**, 1239–1242.

2 W. M. Kluwe, C. A. Montgomery, H. D. Giles and J. D. Prejean, *Food Chem. Toxicol.*, 1983, **21**, 245–250.

3 V. J. Feron, H. P. Til, F. de Vrijer, R. A. Woutersen, F. R. Cassee and P. J. van Bladeren, *Mutat. Res. Toxicol.*,

1991, **259**, 363–385.
4 S. Takeuchi, M. Kochi, K. Sakaguchi, K. Nakagawa and T. Mizutani, *Agric. Biol. Chem.*, 1978, **42**, 1449–1451.
5 M. Kochi, S. Takeuchi, T. Mizutani, K. Mochizuki, Y. Matsumoto and Y. Saito, *Cancer Treat. Rep.*, 1980, **64**, 21–3.
6 K. Ariyoshi-Kishino, K. Hashimoto, O. Amano, J. Saitoh, M. Kochi and H. Sakagami, *Anticancer Res.*, 2010, **30**, 5069–76.
7 H. Sakagami, K. Asano, K. Fukuchi, K. Gomi, H. Ota, K. Kazama, S. Tanuma and M. Kochi, *Anticancer Res.*, **11**, 1533–8.
8 A. Ishida, N. Miwa and S. Mizuno, *Cancer Res.*, 1983, **43**, 4216–4220.
9 H. Ochiai, S. Niwayama and K. Masuyama, *J. Cancer Res. Clin. Oncol.*, 1986, **112**, 216–220.
10 T. Miyakawa, J.-L. Zundel and K. Sakaguchi, *Biochem. Biophys. Res. Commun.*, 1979, **87**, 1024–1030.
11 K. Sakaguchi, T. Miyakawa, S. Takeuchi, K. Nakagawa and E. Hayase, *Agric. Biol. Chem.*, 1979, **43**, 1775–1777.
12 J. M. Dornish, E. O. Pettersen, R. Oftebro and J.-E. Melvik, *Eur. J. Cancer Clin. Oncol.*, 1984, **20**, 1287–1293.
13 M. Watanuki and K. Sakaguchi, *Cancer Res.*, 1980, **40**, 2574–9.
14 T. Tabatabaie and R. A. Floyd, *Toxicol. Appl. Pharmacol.*, 1996, **141**, 389–393.
15 Z. Ulker, L. Alpsoy and A. Mihmanli, *Hum. Exp. Toxicol.*, 2013, **32**, 858–864.
16 C. von Sonntag, *Free-Radical-Induced DNA Damage and Its Repair - A Chemical Perspectiva*, Springer, 2006.
17 S. M. Pimblott and J. A. LaVerne, *J. Phys. Chem. A*, 1997, **101**, 5828–5838.
18 X. Ren, E. Wang, A. D. Skitnevskaya, A. B. Trofimov, K. Gokhberg and A. Dorn, *Nat. Phys.*, 2018, **14**, 1062–1066.
19 X. Ren, E. J. Al Maalouf, A. Dorn and S. Denifl, *Nat. Commun.*, 2016, **7**, 11093.
20 B. Boudaïffa, P. Cloutier, D. Hunting, M. A. Huels and L. Sanche, *Science*, 2000, **287**, 1658–1660.
21 E. Alizadeh and L. Sanche, *Chem. Rev.*, 2012, **112**, 5578–5602.
22 I. Baccarelli, I. Bald, F. A. Gianturco, E. Illenberger and J. Kopyra, *Phys. Rep.*, 2011, **508**, 1–44.
23 J. D. Gorfinkiel and S. Ptasińska, *J. Phys. B At. Mol. Opt. Phys.*, 2017, **50**, 182001.
24 Z. Li, A. R. Milosavljević, I. Carmichael and S. Ptasińska, *Phys. Rev. Lett.*, 2017, **119**, 053402.
25 E. M. Zeman, in *Clinical Radiation Oncology: Fourth Edition*, Elsevier, 2015.
26 R. Meißner, J. Kočišek, L. Feketeová, J. Fedor, M. Fárník, P. Limão-Vieira, E. Illenberger and S. Denifl, *Nat. Commun.*, 2019, **10**, 2388.
27 J. Rak, L. Chomicz, J. Wiczk, K. Westphal, M. Zdrowowicz, P. Wityk, M. Żyndul, S. Makurat and Ł. Golon, *J. Phys. Chem. B*, 2015, **119**, 8227–8238.
28 J. Rackwitz, J. Kopyra, I. Dąbkowska, K. Ebel, M. L. Ranković, A. R. Milosavljević and I. Bald, *Angew. Chemie Int. Ed.*, 2016, **55**, 10248–10252.
29 R. Schürmann, T. Tsering, K. Tanzer, S. Denifl, S. V. K. Kumar and I. Bald, *Angew. Chemie Int. Ed.*, 2017, **56**, 10952–10955.
30 A. Buonaugurio, X. Zhang, S. T. Stokes, Y. Wang, G. B. Ellison and K. H. Bowen, *Int. J. Mass Spectrom.*, 2015, **377**, 278–280.
31 J. Hacaloglu, A. Gokmen, S. Suzer, E. Illenberger and H. Baumgartel, *J. Phys. Chem.*, 1989, **93**, 7095–7098.
32 A. Modelli and P. D. Burrow, *J. Phys. Chem.*, 1984, **88**, 3550–3554.
33 G. R. De Maré, T. Lehman and M. Termonia, *J. Chem. Thermodyn.*, 1973, **5**, 829–832.
34 S. Denifl, S. Ptasińska, B. Sonnweber, P. Scheier, D. Liu, F. Hagelberg, J. Mack, L. T. Scott and T. D. Märk, *J. Chem. Phys.*, 2005, **123**, 104308.
35 D. Klar, M. W. Ruf and H. Hotop, *Int. J. Mass Spectrom.*, 2001, **205**, 93–110.
36 L. G. Christophorou and J. K. Olthoff, *Int. J. Mass Spectrom.*, 2001, **205**, 27–41.
37 M. M. Dawley and S. Ptasińska, *Int. J. Mass Spectrom.*, 2014, **365**–**366**, 143–151.
38 M. J. Frisch, G. W. Trucks, H. B. Schlegel, G. E. Scuseria, M. A. Robb, J. R. Cheeseman, G. Scalmani, V. Barone, G. A. Petersson, H. Nakatsuji, X. Li, M. Caricato, A. V Marenich, J. Bloino, B. G. Janesko, R. Gomperts, B. Mennucci, H. P. Hratchian, J. V Ortiz, A. F. Izmaylov, J. L. Sonnenberg, D. Williams-Young, F. Ding, F. Lipparini, F. Egidi, J. Goings, B. Peng, A. Petrone, T. Henderson, D. Ranasinghe, V. G. Zakrzewski, J. Gao, N. Rega, G. Zheng, W. Liang, M. Hada, M. Ehara, K. Toyota, R. Fukuda, J. Hasegawa, M. Ishida, T. Nakajima, Y. Honda, O. Kitao, H. Nakai, T. Vreven, K. Throssell, J. A. Montgomery Jr., J. E. Peralta, F. Ogliaro, M. J. Bearpark, J. J. Heyd, E. N. Brothers, K. N. Kudin, V. N. Staroverov, T. A. Keith, R. Kobayashi, J. Normand, K. Raghavachari, A. P. Rendell, J. C. Burant, S. S. Iyengar, J. Tomasi, M. Cossi, J. M. Millam, M. Klene, C. Adamo, R. Cammi, J. W. Ochterski, R. L. Martin, K. Morokuma, O. Farkas, J. B. Foresman and D. J. Fox, 2009, Gaussian Inc. Wallingford CT.
39 A. D. Becke, *J. Chem. Phys.*, 1993, **98**, 5648–5652.
40 T. H. Dunning, *J. Chem. Phys.*, 1989, **90**, 1007–1023.
41 A. M. Scheer and P. D. Burrow, *J. Phys. Chem. B*, 2006, **110**, 17751–17756.
42 K. Takatsuka and V. McKoy, *Phys. Rev. A*, 1981, **24**, 2473–2480.
43 K. Takatsuka and V. McKoy, *Phys. Rev. A*, 1984, **30**, 1734–1740.
44 G. B. Bachelet, D. R. Hamann and M. Schlüter, *Phys. Rev. B*, 1982, **26**, 4199–4228.
45 L. M. Cornetta, K. Coutinho, S. Canuto and M. T. d. N. Varella, *Eur. Phys. J. D*, 2016, **70**, 176.
46 F. Kossoski, M. H. F. Bettega and M. T. do N. Varella, *J. Chem. Phys.*, 2014, **140**, 024317.

47 F. Kossoski and M. T. do N. Varella, *Phys. Chem. Chem. Phys.*, 2015, **17**, 17271–17278.
48 P. Skurski, M. Gutowski and J. Simons, *Int. J. Quantum Chem.*, 2000, **80**, 1024–1038.
49 L. A. Curtiss, P. C. Redfern and K. Raghavachari, *J. Chem. Phys.*, , DOI:10.1063/1.2770701.
50 I. Fdez. Galván, M. Vacher, A. Alavi, C. Angeli, F. Aquilante, J. Autschbach, J. J. Bao, S. I. Bokarev, N. A. Bogdanov, R. K. Carlson, L. F. Chibotaru, J. Creutzberg, N. Dattani, M. G. Delcey, S. S. Dong, A. Dreuw, L. Freitag, L. M. Frutos, L. Gagliardi, F. Gendron, A. Giussani, L. González, G. Grell, M. Guo, C. E. Hoyer, M. Johansson, S. Keller, S. Knecht, G. Kovačević, E. Källman, G. Li Manni, M. Lundberg, Y. Ma, S. Mai, J. P. Malhado, P. Å. Malmqvist, P. Marquetand, S. A. Mewes, J. Norell, M. Olivucci, M. Oppel, Q. M. Phung, K. Pierloot, F. Plasser, M. Reiher, A. M. Sand, I. Schapiro, P. Sharma, C. J. Stein, L. K. Sørensen, D. G. Truhlar, M. Ugandi, L. Ungur, A. Valentini, S. Vancoillie, V. Veryazov, O. Weser, T. A. Wesołowski, P.-O. Widmark, S. Wouters, A. Zech, J. P. Zobel and R. Lindh, *J. Chem. Theory Comput.*, , DOI:10.1021/acs.jctc.9b00532.
51 P.-O. Widmark, P.-Å. Malmqvist and B. O. Roos, *Theor. Chim. Acta*, 1990, **77**, 291–306.
52 R. Pou-Amérigo, M. Merchán and E. Ortí, *J. Chem. Phys.*, 1999, **110**, 9536–9546.
53 R. Pou-Amérigo, L. Serrano-Andrés, M. Merchán, E. Ortí and N. Forsberg, *J. Am. Chem. Soc.*, 2000, **122**, 6067–6077.
54 L. Klasinc, B. Kovac and H. Gusten, *Pure Appl. Chem.*, 1983, **55**, 289–298.
55 G. B. Tolstorozhev, I. V. Skornyakov, M. V. Bel'kov, O. I. Shadyro, S. D. Brinkevich and S. N. Samovich, *Opt. Spectrosc.*, 2012, **113**, 179–183.
56 I. Bald, J. Langer, P. Tegeder and O. Ingólfsson, *Int. J. Mass Spectrom.*, 2008, **277**, 4–25.
57 S. Ptasińska, S. Denifl, B. Mróz, M. Probst, V. Grill, E. Illenberger, P. Scheier and T. D. Märk, *J. Chem. Phys.*, 2005, **123**, 124302.
58 P. D. Burrow, G. A. Gallup, A. M. Scheer, S. Denifl, S. Ptasinska, T. Märk and P. Scheier, *J. Chem. Phys.*, 2006, **124**, 124310.
59 S. Denifl, S. Ptasińska, G. Hanel, B. Gstir, M. Probst, P. Scheier and T. D. Märk, *J. Chem. Phys.*, 2004, **120**, 6557–6565.
60 T. Sommerfeld, *J. Phys. Chem. A*, 2004, **108**, 9150–9154.
61 D. Huber, M. Beikircher, S. Denifl, F. Zappa, S. Matejcik, A. Bacher, V. Grill, T. D. Märk and P. Scheier, *J. Chem. Phys.*, 2006, **125**, 084304.
62 S. Gohlke, H. Abdoul-Carime and E. Illenberger, *Chem. Phys. Lett.*, 2003, **380**, 595–599.
63 J. Ameixa, E. Arthur-Baidoo, R. Meißner, S. Makurat, W. Kozak, K. Butowska, F. Ferreira da Silva, J. Rak and S. Denifl, *J. Chem. Phys.*, 2018, **149**, 164307.
64 F. Kossoski, J. Kopyra and M. T. do N. Varella, *Phys. Chem. Chem. Phys.*, 2015, **17**, 28958–28965.
65 F. Ferreira da Silva, M. T. do N. Varella, N. C. Jones, S. Vrønning Hoffmann, S. Denifl, I. Bald and J. Kopyra, *Chem. - A Eur. J.*, 2019, **25**, 5498–5506.
66 S. Ptasińska, S. Denifl, V. Grill, T. D. Märk, E. Illenberger and P. Scheier, *Phys. Rev. Lett.*, 2005, **95**, 093201.
67 A. S. Barbosa and M. H. F. Bettega, *J. Chem. Phys.*, 2017, **146**, 154302.
68 E. M. De Oliveira, S. D. A. Sanchez, M. H. F. Bettega, A. P. P. Natalense, M. A. P. Lima and M. T. D. N. Varella, *Phys. Rev. A - At. Mol. Opt. Phys.*, , DOI:10.1103/PhysRevA.86.020701.